Chemical Research in Toxicology

pubs.acs.org/crt

Article

Investigation of the Interaction between Human Serum Albumin and Branched Short-Chain Perfluoroalkyl Compounds

Giulia Moro, Stefano Liberi, Filippo Vascon, Sara Linciano, Sofia De Felice, Silvano Fasolato, Carlo Foresta, Luca De Toni, Andrea Di Nisio, Laura Cendron,* and Alessandro Angelini*

Cite This: https://doi.org/10.1021/acs.chemrestox.2c00211

Read Online

ACCESS | Metrics & More | Article Recommendations | Supporting Information

ABSTRACT: The current trend dealing with the production of per- and polyfluoroalkyl substances (PFASs) involves the shifting toward branched short-chain fluorinated compounds known as new-generation PFASs. A key aspect to be clarified, to address the adverse health effects associated with the exposure to PFASs, is their binding mode to human serum albumin (hSA), the most abundant protein in plasma. In this study, we investigated the interaction between hSA and two representative branched short-chain PFASs, namely, HPFO-DA and C6O4. In-solution studies revealed that both compounds bind hSA with affinities and stoichiometries lower than that of the legacy long-chain perfluoroalkyl compound PFOA. Competition experiments using hSA-binding drugs with known site-selectivity revealed that both HPFO-DA and C6O4 bound to pockets located in subdomain IIIA. The crystal structure of hSA in complex with HPFO-DA unveiled the presence of two binding sites. The characterization and direct comparison of hSA interactions with new-generation PFASs may be key elements for the understanding of the toxicological impact of these compounds.

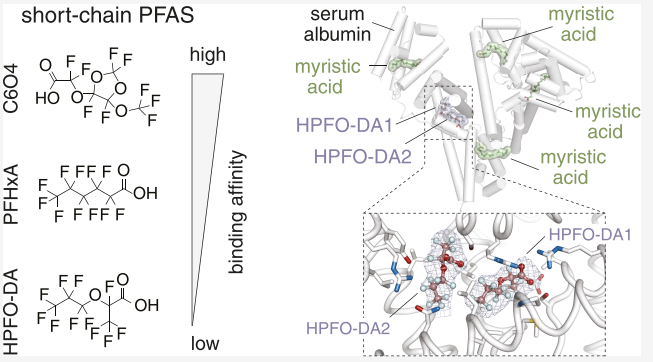

1. INTRODUCTION

Per- and polyfluoroalkyl substances (PFASs) represent a large class of synthetic compounds that comprise a linear or branched carbon chain.[1−4] PFASs are divided into long- and short-chain compounds based on the length of their fully or partially fluorinated carbon chain.[5,6] Long-chain PFASs possess a six or more-perfluorinated carbon backbone, while short-chain ones have less than six perfluorinated carbons.[5,6] The most common long-chain PFASs are perfluorooctanoic acid (PFOA) and perfluorooctanesulfonic acid (PFOS).[6−8] Both PFOA and PFOS are characterized by a high chemical stability, accounting for their widespread use in manufacturing and consumer goods.[9−11] However, the high resistance to degradation allowed them to persist in multiple environmental matrices and bioaccumulate within living organisms with harmful consequences to animal and human health.[12−15] This evidence has ultimately prompted the competent authorities to implement actions aimed at reducing long-chain PFAS production and emissions.[7,16−18]

In response to the strict regulation limits and the phase out actions, short-chain alternatives represent the most attractive targets, from an industry environmental perspective, compared to long-chain PFASs.[19−23] Based on their chemical structure, these alternative fluorinated compounds can be divided into two main categories: perfluoropolyethers with different functional head groups (mainly carboxylic and sulfonic ones) and shorter-chain homologues of long-chain PFASs.[20,24−26] Common short-chain perfluoropolyether replacements are 2,3,3,3-tetrafluoro-2-(heptafluoropropoxy) propanoic acid (HPFO-DA), also known as GenX,[27] and perfluoro ([5-methoxy-1,3-dioxolan-4-yl]oxy) acetic acid (C6O4).[28] HPFO-DA was initially introduced as a safer alternative of PFOA and widely applied in manufacturing.[29] Since its introduction, the environmental impact of HPFO-DA was carefully monitored and its adverse effects on human health found to be similar to those of PFOA and PFOS.[26,30] These findings led the U.S. Environmental Protection Agency and other competent authorities to develop large-scale monitoring plans and declare HPFO-DA a potential carcinogenic agent.[17,31] Oppositely, less information is available regarding C6O4, an alternative to long-chain PFASs, which was considered safe for use in food contact materials by the European Food Safety Agency,[32] and has shown less toxicity in various cell models in vitro.[33,34]

Major health effects of long-chain PFASs are associated with their low elimination rates and high accumulation levels in the

Received: June 30, 2022

blood and in vital organs.[35] Indeed, the average half-life values for serum elimination of legacy PFASs, such as PFOA and PFOS, in environmentally exposed human populations are estimated to be in the order of 1−5 years, depending on the type of compound.[36,37] Such long persistence and accumulation of long-chain PFASs in circulation have been ascribed to their ability to bind human serum albumin (hSA), the most abundant protein in plasma with a maximum circulatory half-life of 19 days in humans.[38,39] hSA can bind a large diversity of PFASs, shielding their hydrophobic character and strongly enhancing their absorption and distribution throughout the body ultimately leading to relatively high blood concentration.[40] While considerable insights into the binding mode of several long-chain PFASs with hSA have been described over the last years,[40−45] a detailed analysis of the interaction of new-generation PFASs with hSA has not been reported yet.

In the present study, we applied isothermal titration calorimetry (ITC) and X-ray crystallography to characterize the interaction of hSA with two representative branched short-chain perfluoropolyethers, namely HPFO-DA and C6O4. Competition experiments with known hSA-binding drugs revealed that both compounds bound to pockets located in a single subdomain. The crystal structure of hSA in complex with HPFO-DA unveiled the presence of two binding sites. The elucidation of the molecular basis of the interaction between hSA and short-chain PFAS alternatives is expected to provide a better assessment of the absorption and elimination processes of these toxic compounds in vivo.

2. MATERIALS AND METHODS

2.1. Proteins and Chemicals. Recombinant human serum albumin, Albagen XL solution (UniProt ID: P02768) was purchased from Albumin Bioscience (Huntsville, AL, USA). The charcoal was purchased from Caesar & Loretz GmbH (Hilden, Germany). Hexafluoropropylene oxide-dimer acid (HFPO-DA or GenX) was purchased from SynQuest Laboratories (Alachua, FL, USA). C6O4 was purchased from Wellington laboratories (Ontario, Canada). Perfluorohexanoic acid (PFHxA), sodium myristate (Myr), and warfarin (War) were purchased from (Merck, Milan, Italy). Ibuprofen (Ibu) was purchased from Cayman Chemical (Ann Arbor, MI, USA). All the reagents were of analytical grade, and solutions were prepared using double distilled deionized water.

2.2. Protein Preparation and Purification. The defatted recombinant human serum albumin (dhSA) was obtained by adsorption onto activated charcoal as previously described.[46,47] Briefly, the water-washed charcoal (0.4 mg per mg of hSA) was initially dissolved in PBS pH 7.4, and the pH was further lowered to 3 using a 1 M HCl solution. The resulting suspension was incubated for at least 3 hr. under gentle shaking at 4 °C. The pH of the suspension was then adjusted to 7.4 by using a 2 M NaOH solution and filtered using a 0.22 μm membrane filter. The protein aggregates and the disulfide-bridged dimers formed during this treatment were removed by size exclusion chromatography (SEC) using a HiLoad 16/600 Superdex 200 prep grade column (GE Healthcare, Milan, Italy) connected to an ÄKTA pure 25 M system (GE Healthcare, Milan, Italy) equilibrated with 50 mM sodium phosphate buffer (NaPi), 100 mM NaCl, pH 7.4. The fractions containing monomeric dhSA protein were pooled and further concentrated by using 10.000 NMWL Amicon Ultra-15 ultrafiltration devices (Merck, Milan, Italy) at 4000 g and 4 °C on a Heraeus Multifuge X1R centrifuge (Thermo Fisher Scientific, Waltham, MA, USA) to a final protein concentration of 25 mg/mL (375 μM). Protein concentration was determined using a mySPEC spectrophotometer (VWR, Radnor, PA, USA). Purified dhSA protein was flash-frozen in liquid nitrogen and stored at −80 °C. The monodisperse state of concentrated dhSA protein was confirmed by SEC using a Superdex 200 10/300 GL column (GE Healthcare, Milan, Italy) connected to an ÄKTA pure 25 M system and equilibrated with 50 mM NaPi, 100 mM NaCl, pH 7.4. Purified dhSA proteins were eluted as a single peak at elution volumes that corresponds to an apparent molecular mass of about 66 kDa (monomer).

2.3. Isothermal Titration Calorimetry. ITC experiments were performed using a Microcal PEAQ-ITC instrument (Malvern Panalytical, Malvern, UK). Both dhSA (110 μM) and ligands (HPFO-DA, C6O4, PFHxA, Ibu, and War, 4 mM solutions) were dissolved in 50 mM NaPi, 100 mM NaCl, pH 7.4. Only in the case of War, 2.5% v/v DMSO was added to the buffer to improve its solubility. All working solutions were properly degassed. Titrations of dhSA with ligands were carried out at different temperatures (298 and 310 K). In each experiment, an initial 0.4 μL injection (excluded from subsequent data analysis) was followed by 25 independent injections of 1.5 μL with a stirring rate of 750 rpm to ensure rapid mixing. A 120 s interval between injections was applied to guarantee the equilibrium at each titration point. Blank experiments (ligands against buffer) were carried out for each ligand and subtracted to corresponding titrations in order to screen dilution heat contributions. Competition experiments were conducted by adding saturating concentrations of albumin-binding drugs (either 250 μM Ibu or 200 μM War) to dhSA in the measure cell and titrating each PFAS (4 mM) with the aforementioned instrumental parameters. Data were analyzed using the MicroCal PEAQ-ITC Evaluation software (Malvern Panalytical, Malvern, UK). Integrated heat signals were fitted to "one set of sites" (C6O4, PFHxA), "two sets of sites" (PFOA), or "sequential" (HPFO-DA) binding models. Values for the binding affinity constant ($K_A = 1/K_D$) and enthalpy change (ΔH), together with the stoichiometry of each PFAS-dhSA reaction, were obtained from curve fitting. Free energy and the entropy change (ΔS) were calculated from the Gibbs free energy (ΔG) relationships: $\Delta G = \Delta H - T\Delta S = -RT \ln(K_A)$.

2.4. Crystallization. Crystallization trials of dhSA in complex with HPFO-DA, C6O4 and sodium myristate (Myr) were carried out at 285 K in an MRC maxi 48-well crystallization plate (Hampton Research, Aliso Viejo, CA, USA) using the sitting-drop vapor-diffusion method and the Morpheus MD1−46 protein crystallization screen kit (Molecular Dimensions Ltd., Catcliffe, UK). Droplets of 1.6 μL volume (0.8 μL of protein complex and 0.8 μL of reservoir solution) were set up using an Oryx 8 crystallization robot (Douglas Instruments Ltd., Catcliffe, UK) and equilibrated against 120 μL reservoir solution. In all the cases, best crystals were obtained by streak- or micro-seeding and left for 5−7 days. Crystals of dhSA (1 mM) incubated with a 20-fold molar excess of HPFO-DA (20 mM) and a fivefold molar excess of Myr (5 mM) were obtained using the following precipitant agents: 50 mM bicine, 50 mM Trizma base, 30 mM sodium fluoride, 30 mM sodium bromide, 30 mM sodium iodide, 12.5% v/v MPD, 12.5% w/v PEG 1000, and 12.5% w/v PEG 3350 pH 8.5. For X-ray data collection, crystals were mounted on LithoLoops (Molecular Dimensions Ltd., Catcliffe, UK), soaked in cryoprotectant solution (crystallization buffer added with 20% v/v ethylene glycol), and flash-frozen in liquid nitrogen.

2.5. X-ray Diffraction Data Collection and Processing. X-ray diffraction data of the complexes were collected at ID23−2 beamline of the European Synchrotron Radiation Facility (ESRF, Grenoble, France). The best crystals of the ternary complex hSA-HPFO-DA-Myr (1:20:5 molar ratio) diffracted to 2.10 Å maximum resolution. Crystals belong to the C2 space group, with unit cell parameters: a = 185.89 Å, b = 38.77 Å, c = 96.45 Å, α = 90°, β = 105°, and γ = 90°. The asymmetric unit contains one molecule, corresponding to a Matthews coefficient of 2.45 Å^3/Da and a solvent content of 49.84% of the crystal volume. Frames were indexed and integrated with software XIA2, merged, and scaled with AIMLESS (CCP4i2 crystallographic package).[48]

2.6. Structure Determination and Model Refinement. The structure was solved by molecular replacement with software PHASER[49] using as a template the model 7AAI.[45] Refinement was carried on using REFMAC[50] and PHENIX.[51] Rebuilding and fitting of the HPFO-DA, Myr, and precipitant/additive molecules (2-methyl-2,4-pentanediol, MPD; and Br) were performed manually with

https://doi.org/10.1021/acs.chemrestox.2c00211
Chem. Res. Toxicol. XXXX, XXX, XXX−XXX

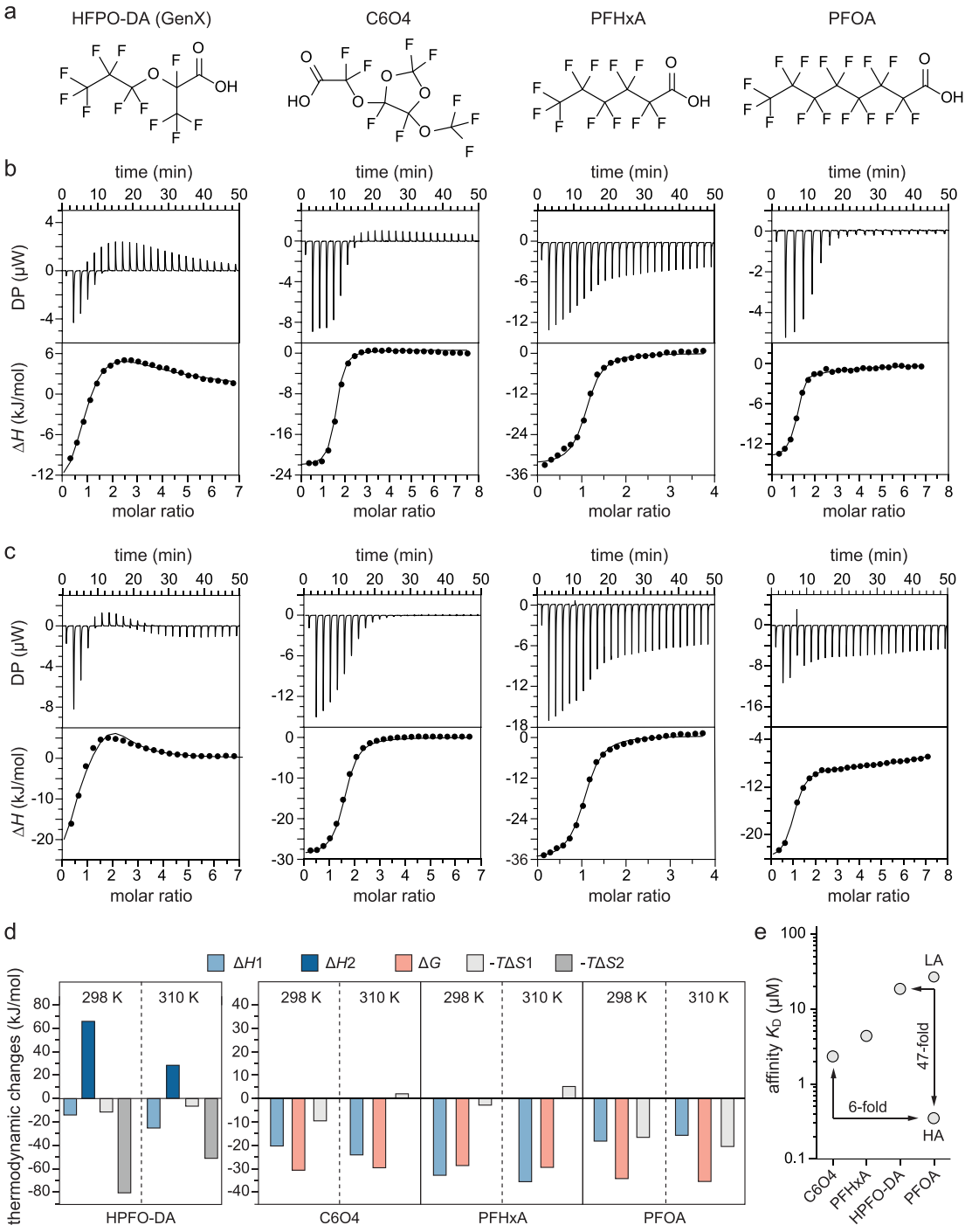

Figure 1. Binding kinetics of branched short-chain HPFO-DA and C6O4 to hSA compared to those of linear PFHxA (short-chain) and PFOA (long-chain) to hSA. (a) Chemical structure of HPFO-DA, C6O4, PFHxA, and PFOA; (b, c) ITC analysis of hSA binding to PFASs performed at two different temperatures. Representative raw trace (top) and integrated binding isotherm (bottom) of the calorimetric titration of HPFO-DA, C6O4, PFHxA, and PFOA at 298 K (b) and 310 K (c); (d) comparative analysis of the thermodynamic parameters: bar diagram representing the difference in enthalpy ($\Delta H1$ and $\Delta H2$, light and dark blue), in free Gibson energy (ΔG, light red) and entropy ($-T\Delta S1$ and $-T\Delta S2$, light and dark gray) for each dhSA-PFAS complex according to the fitting selected (sequential binding for HPFO-DA, one set of sites for C6O4 and PFHxA and two sets of sites for PFOA). For PFOA, only the parameters describing the high-affinity sites are reported; (e) summary of the K_D values (light gray) of HPFO-DA, C6O4, PFHxA, PFOA-HA (HA = high-affinity binding sites) and PFOA-LA (LA = low-affinity binding sites) at 298 K.

graphic software COOT.[52] Since the first cycles of refinement, the electron density corresponding to the bound HPFO-DA and/or Myr molecules was clearly visible in the electron density map. The final model of the ternary complex hSA-HPFO-DA-Myr contains 4643 protein atoms, 40 HPFO-DA ligand atoms, 64 Myr ligand atoms, 34 water molecules, and 49 atoms of other molecules. The final crystallographic R factor is 0.237 (R_{free} 0.264). Geometrical parameters of the two models are as expected or better for this resolution. Intramolecular and intermolecular hydrogen bond interactions were analyzed by PROFUNC,[53] LIGPLOT+,[54] and

https://doi.org/10.1021/acs.chemrestox.2c00211
Chem. Res. Toxicol. XXXX, XXX, XXX−XXX

PYMOL software.[55] The Protein Data Bank (PDB) identification code for the hSA-HPFO-DA-Myr ternary complex is 7Z57.

3. RESULTS AND DISCUSSION

3.1. Binding Kinetics of Branched Short-Chain HPFO-DA and C6O4 with hSA. To determine the binding affinities of branched short-chain HPFO-DA and C6O4 to hSA, we used ITC. In-solution studies were performed at room (298 K) and physiological (310 K) temperatures. Linear long- and short-chain perfluoroalkyl compound PFOA and PFHxA, respectively, were included as controls (Figure 1a). Linear PFHxA was chosen because it contains the same number of perfluorinated carbons of both branched short-chain HFPO-DA and C6O4. PFOA was instead selected because it represents the prototype of perfluoropolyethers with a carboxylic head, and it is one of the most widely studied perfluoroalkyl substances. The binding mode of branched C6O4 to hSA resembled that of linear PFHxA (Figure 1b). Both short-chain PFASs appear to form stable complexes with hSA presenting similar binding affinity constants (C6O4: K_D = 2.4 ± 0.1 μM; PFHxA: K_D = 4.5 ± 2.1 μM; Figure 1b,c and Table 1). Binding isotherms at 298 and 310 K were best fitted with a "one set of sites" model revealing a 1:2 and 1:1 hSA:PFAS stoichiometry for C6O4 and PFHxA, respectively (Figure 1b,c and Table 1). Their binding kinetics are characterized by an exothermic reaction with favorable enthalpic (ΔH) and entropic (ΔS) contributions, suggesting that the formation of both hSA-C6O4 and hSA-PFHxA complexes is achieved through electrostatic and hydrophobic contacts (Figure 1d and Table 1). Inversely, binding of branched HPFO-DA to hSA was best fitted using a "sequential binding" model, with a first high-affinity binding event (K_D = 19 ± 1.3 μM) followed by a second lower affinity one (K_D > 80 μM; Figure 1b,c and Table 1). The initial binding event resembled that of the three low-affinity binding sites of PFOA (K_D = 29.7 ± 1.7 μM; Figure 1b,c and Table 1). The second binding event could instead be plausibly attributed to unspecific hydrophobic interactions occurring at high HPFO-DA concentrations. Indeed, this hypothesis is supported by the fact that the first binding event is enthalpically favored ($-T\Delta S$ = −12.9 ± 4.7; ΔH = −14.1 ± 4.9 kJ/mol), while the second binding event appears to be primarily entropically driven (ΔH = 33.8 kJ/mol; $-T\Delta S$ = −57.1 kJ/mol; Figure 1d and Table 1). Notably, no significant variations were observed in the stoichiometry nor in the binding affinities when ITC studies were performed at temperatures of 298 or 310 K (Figure 1b−d and Table 1). Overall, our in-solution binding studies revealed that, though some differences exist in the biding mechanisms and thermodynamic profiles of herein tested branched and linear short-chain PFASs, all three tested perfluorinated compounds have a weaker affinity for hSA than PFOA (Figure 1e and Table 1).

Table 1. Thermodynamic and Stoichiometric Data for the Binding of dhSA to HPFO-DA, C6O4, PFHxA at Different Temperatures (298 and 310 K)[a]

one set of sites				
	C6O4		PFHxA	
	298 K	310 K	298 K	310 K
K_D (μM)	2.4 ± 0.1	5.4 ± 2.1	4.5 ± 2.10	5.9 ± 0.70
ΔH (kJ/mol)	−21.4 ± 1.4	−25.8 ± 4.2	−34.1 ± 7.40	−39.2 ± 2.00
ΔG (kJ/mol)	−32.10	−31.70	−30.60	−31.70
$-T\Delta S$ (kJ/mol)	−10.7	1.7	−3.00	7.70
n	1.6 ± 0.2	1.5 ± 0.3	1.02 ± 0.05	1.03 ± 0.05
sequential binding				
	HPFO-DA			
	298 K	310 K		
K_{D1} (μM)	19.0 ± 1.3	9.9 ± 2.3		
ΔH_1 (kJ/mol)	−14.1 ± 4.9	−23.2 ± 3.4		
$-T\Delta S_1$ (kJ/mol)	−12.9	−6.54		
K_{D2} (μM)	84.2 ± 14.6	27.0 ± 8.1		
ΔH_2 (kJ/mol)	33.8 ± 1.9	28.2 ± 2.8		
$-T\Delta S_2$ (kJ/mol)	−57.1	−55.4		
two sets of sites				
	PFOA high-affinity sites		PFOA low-affinity sites	
	298 K	310 K	298 K	310 K
K_D (μM)	0.4 ± 0.01	39.3 ± 0.4	29.7 ± 1.7	46.0 ± 2.00
ΔH (kJ/mol)	−20.1 ± 1.10	−16.5 ± 1.9	−20.1 ± 1.1	−2.26 ± 0.75
ΔG (kJ/mol)	−36.10	−38.10	−26.60	−29.10
$-T\Delta S$ (kJ/mol)	−17.70	−21.6	−28.2	−31.30
n	0.89 ± 0.30	0.95 ± 0.2	4.5 ± 1.2	9.5 ± 0.20

[a] K_D, equilibrium dissociation constant; ΔH, enthalpy change; ΔG, Gibbs free energy; ΔS, entropy change; T, temperature; n, stoichiometry. Mean values and error of each parameter have been obtained from the fitting.

3.2. Competition Binding Experiments Using Drugs with Known hSA Site-Selectivity. To assign the binding pockets of each branched short-chain PFAS, we performed competitive ITC studies using two commercially available drugs with known binding affinities and site-selectivity for hSA.[45] These include ibuprofen (Ibu) and warfarin (War), two well-characterized molecules known to share the same fatty acid-binding sites (FA4 and FA6 for Ibu, FA7 for War) with long-chain PFASs (Figure 2a).[45] Again, the short-chain perfluoroalkyl compound PFHxA was included as the control. Individual titration profiles of perfluorinated compounds HPFO-DA, C6O4, and PFHxA to hSA saturated with War were comparable to that of hSA in the absence of competitive drug, while those obtained in the presence of Ibu-saturated hSA revealed a nearly saturated flat curve, suggesting a direct competition of Ibu with both branched short-chain PFASs for FA4 and/or FA6 binding sites (Figures 2b and S1). The thermodynamics parameters of binding of both branched and linear tested short-chain PFASs to hSA in the presence of Ibu showed little or null enthalpic contribution, which was instead present when the hSA was saturated with War and comparable to that of hSA in the absence of competitive drugs (Figures 2b and S1). The results are consistent with those previously reported that identified the ibuprofen-binding pocket as a preferable cavity to lodge polyfluoroalkyl compounds.[45] Given that all three tested perfluorinated compounds bind hSA with a 1:2 and 1:1 hSA:PFAS stoichiometry and appear to compete with Ibu, we can conclude that HPFO-DA, C6O4 and PFHxA preferably occupy FA4 and/or FA6 sites (Figure 2c).

3.3. Crystal Structure of hSA in Complex with HPFO-DA. To elucidate the binding mode of HPFO-DA and C6O4 to hSA, we applied X-ray crystallography and attempted to solve the three-dimensional structure of both perfluorinated

https://doi.org/10.1021/acs.chemrestox.2c00211
Chem. Res. Toxicol. XXXX, XXX, XXX−XXX

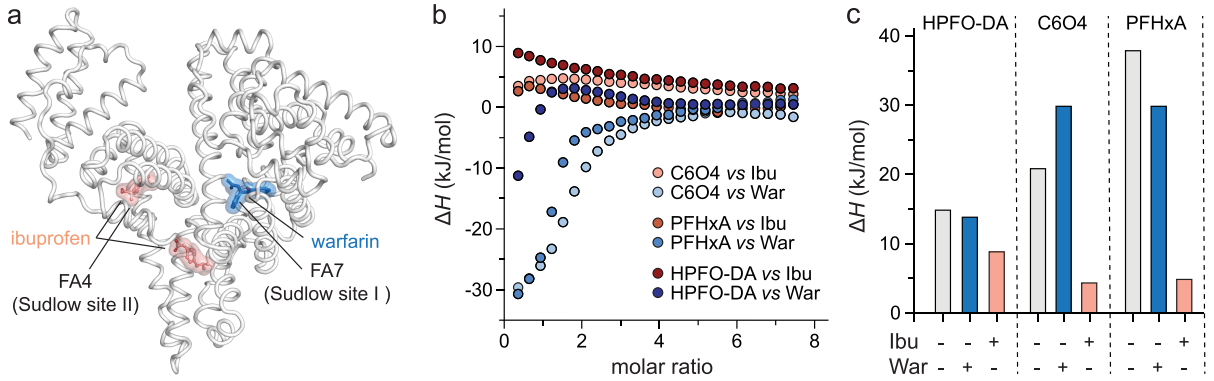

Figure 2. In-solution competitive binding experiments using drugs with known hSA site-selectivity. (a) Structural comparison of the ligand binding modes of ibuprofen (Ibu, salmon) and warfarin (War, sky blue) to hSA (white); (b) overlay of the individual titration profiles of short-chain HPFO-DA, C6O4, and PFHxA biding to hSA saturated with Ibu (red scale) or War (blue scale). The titration profiles are colored in light red and light blue for C6O4, red and blue for PFHxA, and dark red and dark blue for HPFO-DA; (c) difference in enthalpy (ΔH) of the HPFO-DA, C6O4, and PFHxA binding to hSA in absence of competitors (light gray), in the presence of ibuprofen (Ibu, salmon) or in the presence of warfarin (War, blue). The three-dimensional structure was generated and rendered using PYMOL.[55]

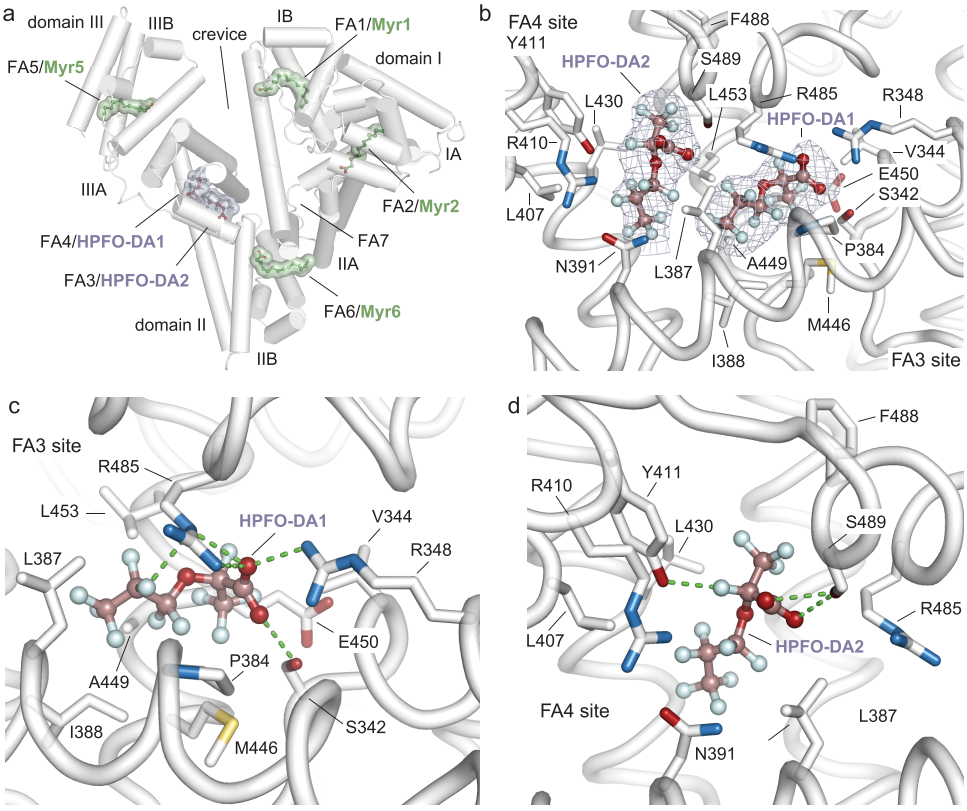

Figure 3. Crystal structure of branched short-chain HPFO-DA in complex with hSA. (a) Three-dimensional structure of hSA (white) in complex with two molecules of HPFO-DA (light purple) and Myr (green) [PDB identification code: 7Z57]. The α-helices of hSA are represented by cylinders. Bound HPFO-DA and Myr molecules are shown in a ball-and-stick representation with a semitransparent van der Waals (HPFO-DA: light purple, Myr: green) and colored by atom type (HPFO-DA: carbon = dark salmon, oxygen = firebrick, fluorine = pale cyan; Myr: carbon = smudge green, oxygen = firebrick); (b) HPFO-DA1 and HPFO-DA2 bound to FA3 and FA4 sites located in subdomain IIIA, respectively. Bound HPFO-DA molecules are depicted as ball-and-stick models and the composite omit maps, representing the ($F_o - F_c$) electron density contoured at 4σ, are shown as light purple mesh.; (c) HPFO-DA1 bound to FA3 site; (d) HPFO-DA2 bound to FA4 site. The α-helices of hSA are shown in white and the selected amino acid side chains are represented as stick and colored by atom type (carbon = white, oxygen = firebrick, nitrogen = sky blue; sulfur = yellow orange). Hydrogen bonds, salt bridges, and polar interactions are shown as dashed lines. For visualization, only intermolecular polar interactions below 3.0 Å are shown. The three-dimensional structures were generated and rendered using PYMOL.[55]

compounds in complex with hSA. To better resemble the physiological conditions, cocrystallization trials were performed in the presence of a representative fatty acid, the myristic acid (Myr).[56] Despite the numerous attempts, good-quality diffraction crystals were obtained only for hSA in complex with HPFO-DA and Myr. The best crystals diffracted to 2.2 Å maximum resolution, and the structure was solved by molecular replacement (Table S1, PDB identification code:

https://doi.org/10.1021/acs.chemrestox.2c00211
Chem. Res. Toxicol. XXXX, XXX, XXX−XXX

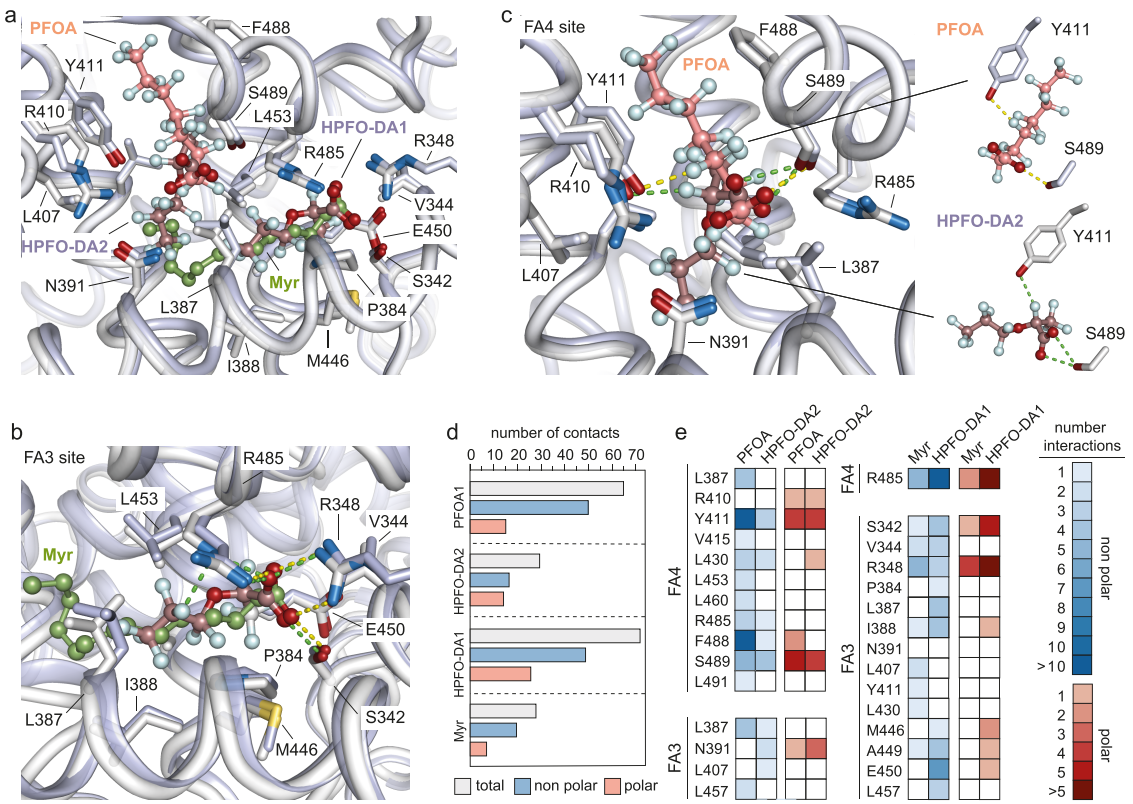

Figure 4. Structural comparison of the ligand binding modes of HPFO-DA and PFOA to hSA. (a) Detailed view of the superimposed PFOA, HPFO-DA1, HPFO-DA2, and Myr ligands bound to FA4 and FA3 sites in subdomain IIIA of hSA; (b) detailed view of the superimposed HPFO-DA1 and Myr ligands bound to the FA3 site; (c) detailed view of the superimposed HPFO-DA2 and PFOA ligands bound to the FA4 site. The α-helices of hSA in complex with PFOA and Myr are represented by light blue ribbon diagram while the α-helices of hSA in complex with HPFO-DA1 and HPFO-DA2 are represented by the white ribbon diagram. The selected amino acid side chains are represented as sticks and colored by the atom type (carbon = white for hSA-HPFO-DA-Myr complex and light blue for hSA-PFOA-Myr complex, oxygen = firebrick, nitrogen = sky blue, sulfur = yellow orange). Bound HPFO-DA, PFOA, Myr molecules are shown in a ball-and-stick representation and colored by the atom type (HPFO-DA: carbon = dirty violet, oxygen = firebrick, fluorine = pale cyan; PFOA: carbon = dark salmon, oxygen = firebrick, fluorine = pale cyan; Myr: carbon = smudge green, oxygen = firebrick). Only the side chains of amino acids of hSA forming intermolecular interactions below 4.0 Å are shown. Polar intermolecular interactions are represented as dashed lines. Those established by HPFO-DAs are colored in light green, while those formed by PFOA or Myr are colored in yellow; (d) columns graph reporting the number of total (light gray), nonpolar (light blue), and polar (light red) intermolecular interactions of hSA with HPFO-DA1, HPFO-DA2, PFOA, and Myr; (e) heat map visualization of the number of interactions of hSA residues involved in binding to HPFO-DA1 and Myr (left), HPFO-DA2 and PFOA (right). The residues of hSA are indicated as a three numbered letter code. Nonpolar interaction and polar interaction are shown in blue and red, respectively. The color intensity correlates with the number of the interactions, with numerous and few interactions shown as light and dark colors, respectively. The three-dimensional structures were generated and rendered using PYMOL.[55]

7Z57). A total of six distinct binding sites, two occupied by HPFO-DA and four by Myr, have been identified (Figure 3a). The electronic density of bound HPFO-DA ligands was clearly visible allowing a definite assignment of the positions and orientations of both hydrophilic carboxylate head groups and fluorinated lipophilic tails (Figure 3b). Both HPFO-DA molecules (herein named HPFO-DA1 and HPFO-DA2) occupy the long and narrow Sudlow's drug-binding site II that span between FA3 and F4 sites, both located in subdomain IIIA (Figure 3a,b). The two molecules are closely located and positioned approximately at right angles to each other (Figure 3a,b). HPFO-DA1 is lying into the FA3 site while HPFO-DA2 lodges the F4 site (Figure 3b). The carboxylate head-group of HPFO-DA1 forms hydrogen bonds with the side chain of Ser342, Arg348, and Arg485 residues (Figure 3c). Furthermore, numerous polar interactions are established between fluorine atoms (F5, F6, F7, F14, F15, and F16) and the oxygen and nitrogen atoms of both main and side chains of nearby Ser342, Pro384, Ile388, Met446, Ala449, Glu450, and Arg485 residues (Figure 3c and Table S2). The rest of the fluorinated tail accommodates in the hydrophobic tunnel and establishes nonpolar contacts with surrounding Ser342, Val344, Arg348, Pro384, Leu387, Ile388, Met446, Ala449, Glu450, Leu453, and Arg485 residues (Figure 3c and Table S2). The hydrophilic carboxylate head-group of HPFO-DA2 is instead engaged in a hydrogen bond with the side chain of Ser489, while numerous polar interactions are established between fluorine atoms (F6, F12, F14, F15, F16, F18, and F19) and the oxygen and nitrogen atoms of both main and side chains of nearby Asn391, Tyr411, Leu430, Phe488, and Ser489 residues (Figure 3d and Table S2). The rest of the fluorinated tail accommodates in the hydrophobic tunnel and establishes nonpolar contacts with surrounding Leu387, Asn391, Leu407, Tyr411, Leu430, Arg485, Phe488, and Ser489 residues (Figure 3d and Table S2). Overall, binding of HPFO-DA molecules to FA3 and FA4 pockets involves both the carboxylate head-group and the fluorinated

https://doi.org/10.1021/acs.chemrestox.2c00211
Chem. Res. Toxicol. XXXX, XXX, XXX−XXX

tail that establish polar and nonpolar contacts with surrounding hSA residues.

3.4. Differences in the Binding Mode of Branched Short-Chain HPFO-DA and Linear Long-Chain PFOA with hSA. We next compared our hSA-HPFO-DA-Myr structure with that of hSA in complex with linear long-chain PFOA molecules (PDB identification code: 7AAI).[41,45] The superposition of the two crystal structure complexes did not show any striking rearrangements of the main backbone with root mean square deviations over Cα-atoms of 0.48 Å (Figure S2). Though hSA amino acid side chains involved in the binding to HPFO-DA1 and HPFO-DA2 superimposed well with those of the hSA-PFOA-Myr complex, some differences appear to exist in the positioning of ligands inside the pockets (Figure 4a). Indeed, while the hSA-HPFO-DA-Myr complex revealed the presence of two HPFO-DA molecules bound to FA3 (HPFO-DA1) and F4 (HPFO-DA2) sites, respectively, the hSA-PFOA-Myr complex identified a single PFOA molecule located in the FA4 site and a Myr one into the FA3 pocket (Figure 4a). Both HPFO-DA1 and Myr in FA3 are positioned approximately at right angles to HPFO-DA2 and PFOA molecules located in the nearby FA4 site, respectively (Figure 4a). The hydrophilic carboxylate head-group and the lipophilic tail of HPFO-DA1 in FA3 superimposed well with that of Myr (Figure 4b). Both HPFO-DA1 and Myr ligands establish polar and nonpolar contacts with similar surrounding main and side chain hSA residues (Figure 4b). Most of the hSA side chains that are engaged in HPFO-DA1 binding displayed similar conformations of the hSA-PFOA-Myr complex except for a slight rotation of the Leu387 side chain (Figure 4b). Contrariwise, the binding mode of HPFO-DA2 and PFOA ligands to the FA4 site varies significantly (Figure 4b). While the hydrophilic head groups converge toward a common central polar residue (Ser489), with whom they establish a polar interaction, the fluorinated tails run in opposite directions exploiting different hSA residues (Figure 4c). Notably, F19 and F12 atoms of HPFO-DA1 and PFOA, respectively, establish similar fluorine polar interaction with Tyr411 (Figure 4c). Again, no major differences are observed for the position of side chains of hSA amino acids involved in contacts with HPFO-DA2 when compared to the hSA-PFOA complex (Figure 4c). Interestingly, molecular analysis of the intermolecular interactions established by HPFO-DA1 and HPFO-DA2 with surrounding hSA residues of FA3 and F4 pockets, respectively, revealed that HPFO-DA1 forms a larger number of polar and nonpolar contacts if compared to HPFO-DA2 (Figure 4d,e). Overall, we conclude that HPFO-DA1 appears to bind to FA3 similarly to Myr, while HPFO-DA2 occupies the FA4 site by exploiting different locations and hSA residues.

4. DISCUSSION AND CONCLUSIONS

Exposure of general population to PFASs occurs, in most cases, through oral ingestion of contaminated food or drinking water. After absorption in the gut, PFASs reach the bloodstream and distribute throughout the body, accumulating in certain organs or tissues. This latter event ultimately associates with adverse health outcomes. While the interaction of hSA with linear long-chain PFASs, such as PFOA and PFOS, has been already characterized using multiple methodologies, a detailed analysis of the binding mode of new-generation short-chain polyfluoroalkyl compounds to hSA is still lacking. Here, we report the biochemical characterization of hSA in complex with representative branched short-chain fluorinated compounds HPFO-DA and C6O4. In-solution ITC binding studies revealed the presence of one to two hSA binding sites for both branched short-chain PFASs. Our data are partially in agreement with those reported in previous studies describing the ability of hSA to bind several HPFO-DA molecules.[40,43] The nature of the binding of HPFO-DA and C6O4 to hSA appears to be similar to that of linear short-chain (PFHxA) and long-chain (PFOA) compounds. Binding energetics appear to be driven by an exothermic process and by a gain in entropy most probably due to desolvation of the fluoroalkyl tail. The approximately 6- to 47-fold lower binding affinities determined for short-chain PFASs (C6O4, K_D = 2.4 μM; HPFO-DA, K_D = 19 μM), compared to that of their long-chain counterparts (K_D = 0.4 μM), can be mainly ascribed to their shorter hydrophobic tail that ultimately limit the number of hydrophobic interactions that can be established with the surrounding hSA residues. However, despite these major structural changes, the protein binding affinity of such short-chain PFAS to hSA should be elucidated case by case.[43,57] In particular, given the similar size, we can speculate that the higher binding affinity measured for the C6O4 compound with respect to HPFO-DA and PFHxA could be related to the greater number of oxygen atoms present. Indeed, while HPFO-DA and PFHxA include only two and three oxygens, respectively, C6O4 contains six oxygens that can potentially function as hydrogen bond donors.[28] However, this does not apply to HPFO-DA whose affinity for hSA is weaker than that of PFHxA, despite the presence of an additional oxygen atom. This suggests that the total number of atoms in the backbone might also play a role and that the intermolecular forces at stake are not easy to foresee. Further competition experiments with known hSA-binding drugs identified the Sudlow's drug-binding site II in subdomain IIIA as the high-affinity binding site. The ability of all tested short-chain perfluorinated compounds to outcompete with Ibu for Sudlow's drug-binding site II, a primary site for numerous drugs, is remarkable and supports the need to further investigate the resulting role in PFASs' toxico-kinetics at different levels: from the impact on the serum half-life of the compound, largely ascribed to renal elimination of the "free" form unbound to hSA,[58] to the interference with absorption and accumulation of other exogenous drugs and the related potential toxicity. Indeed, binding of PFASs to hSA, the major drug-carrier protein in blood plasma,[59] might prevent or displace drug binding thus increasing concentration of the unbound drug in circulation, altering its pharmacological effect, and posing health risks. To unveil the molecular basis of the binding mode of both perfluorinated compounds to hSA we attempted to solve the three-dimensional structure of HPFO-DA-hSA and C6O4-hSA complexes. However, while good-quality diffraction crystals were readily attained for hSA in complex with HPFO-DA, no crystals were detected for hSA bound to C6O4 despite the numerous crystallization trials performed. Overall, the crystal structure of hSA in complex with HPFO-DA and Myr revealed the presence of two distinct HPFO-DA binding sites and no conformational differences with those of other hSA-FA complexes. Further comparison of the crystal structure of hSA in complex with HPFO-DA and Myr with that of hSA in complex with PFOA and Myr enabled us to appreciate the analogies and differences in their respective interaction mechanisms. For instance, our structural studies showed that HPFO-DA2 can access a different compartment of FA4 and

https://doi.org/10.1021/acs.chemrestox.2c00211
Chem. Res. Toxicol. XXXX, XXX, XXX−XXX

explore novel hSA amino acids located at the interface between FA3 and FA4 sites otherwise inaccessible. This appears to depend on the presence of the smaller ligand HPFO-DA1 instead of the longer-chain Myr in the FA3 pocket. Indeed, the presence of a sterically bulky Myr that occupies entirely the FA3 pocket of the hSA-PFOA-Myr complex seems to prevent PFOA molecules from entering further deeply center of the pocket leaving it to sit in the middle of FA4 site. Again, our observations partially deviate from those reported in previous studies.[40,42,43,57] While in-solution and structural molecular analysis here presented confirmed the presence of a HPFO-DA molecule (HPFO-DA2) bound to the FA4 site, no HPFO-DA ligand has been shown to bind to the FA7 site (Sudlow's site I). Moreover, contrarily from what was anticipated from computational studies,[44] HPFO-DA molecule positions differently into the FA4 site, and it does not engage in hydrogen bonds with nearby Arg410. Notably, our crystallographic studies unveiled the presence of an unpredicted HPFO-DA molecule (HPFO-DA1) bound to FA3. The ability of the short-chain HPFO-DA molecules to outcompete Myr not only for FA4 but also for FA3 site binding is surprising, especially in light of the fact that neither the long-chain PFOA was found to be able to displace Myr bound to FA3. Indeed, comparative analysis of the interactions of HPFO-DA ligands to the residues of hSA showed that the HPFO-DA1 molecule bound to FA3 establishes a higher number of intermolecular contacts if compared to the HPFO-DA2 molecule bound to FA4. We can speculate that the smaller size of HPFO-DA, with respect to PFOA, might have facilitated its diffusion into the Sudlow's binding sites II (FA3−FA4), a long and narrow hydrophobic tunnel, known to discriminate ligands based on their size. One molecule of HPFO-DA could probably initially penetrate and lodge into the FA3 site followed by a second molecule of HPFO-DA that is instead located into the contiguous FA4 pocket. The simultaneous presence of two molecules of HPFO-DA into the FA3 and FA4 sites might induce a cooperative binding that ultimately contributes to displace the Myr3 situated in FA3. In conclusion, we have demonstrated that new-generation branched short-chain perfluoroalkyl compounds can bind hSA, though with weaker affinity as compared to the long-chain ones. Compared with legacy PFASs, these data support a lower affinity of new-generation PFAS alternatives to hSA, possibly suggesting a lower half-life in vivo, as already reported for HPFO-DA in rodents.[60] However, the global health impact should necessarily consider the specific tissue and cell toxicity that in the case of C6O4 is still under investigation while for HPFO-DA is particularly relevant.[61] Further toxicological and epidemiological studies are needed to address the complete toxicokinetic profile of new-generation alternatives to legacy PFAS.

■ ASSOCIATED CONTENT

Supporting Information

The Supporting Information is available free of charge at https://pubs.acs.org/doi/10.1021/acs.chemrestox.2c00211.

Supplementary tables and supplementary figures, statistics on X-ray diffraction data collection and refinement, atoms of HPFO-DA forming intermolecular polar and nonpolar interactions with atoms and residues of hSA, isothermal titration calorimetry analysis of defatted hSA to HPFO-DA, C6O4, and PFHxA in the presence of hSA-binding drugs ibuprofen or warfarin, and superimposition of hSA-HPFO-DA-Myr and hSA-PFOA-Myr complexes (PDF)

■ AUTHOR INFORMATION

Corresponding Authors

Laura Cendron − *Department of Biology, University of Padua, 35131 Padua, Italy*; Email: laura.cendron@unipd.it

Alessandro Angelini − *Department of Molecular Sciences and Nanosystems, Ca' Foscari University of Venice, 30172 Venice, Italy; European Centre for Living Technology (ECLT), 30123 Venice, Italy;* orcid.org/0000-0001-5923-3843; Email: alessandro.angelini@unive.it

Authors

Giulia Moro − *Department of Molecular Sciences and Nanosystems, Ca' Foscari University of Venice, 30172 Venice, Italy; Department of Medicine, University of Padua, 35128 Padua, Italy*

Stefano Liberi − *Department of Biology, University of Padua, 35131 Padua, Italy;* Present Address: The Armenise-Harvard Laboratory of Structural Biology, Department of Biology and Biotechnology "L. Spallanzani", University of Pavia, Via Ferrata 9, 27100 Pavia, Italy (S.L.)

Filippo Vascon − *Department of Biology, University of Padua, 35131 Padua, Italy*

Sara Linciano − *Department of Molecular Sciences and Nanosystems, Ca' Foscari University of Venice, 30172 Venice, Italy*

Sofia De Felice − *Department of Biology, University of Padua, 35131 Padua, Italy*

Silvano Fasolato − *Department of Medicine, University of Padua, 35128 Padua, Italy*

Carlo Foresta − *Department of Medicine, Unit of Andrology and Reproductive Medicine, University of Padua, 35128 Padua, Italy*

Luca De Toni − *Department of Medicine, Unit of Andrology and Reproductive Medicine, University of Padua, 35128 Padua, Italy*

Andrea Di Nisio − *Department of Medicine, Unit of Andrology and Reproductive Medicine, University of Padua, 35128 Padua, Italy*

Complete contact information is available at: https://pubs.acs.org/10.1021/acs.chemrestox.2c00211

Author Contributions

CRediT: **Giulia Moro** conceptualization, data curation, formal analysis, investigation, methodology, writing-original draft, writing-review & editing; **Stefano Liberi** conceptualization, data curation, formal analysis, investigation, methodology, writing-original draft, writing-review & editing; **Filippo Vascon** data curation, formal analysis, investigation, methodology, writing-review & editing; **Sara Linciano** data curation, formal analysis, investigation, methodology, writing-review & editing; **Sofia De Felice** data curation, formal analysis, investigation, methodology, writing-original draft; **Silvano Fasolato** resources, writing-review & editing; **Carlo Foresta** resources, supervision, writing-review & editing; **Luca De Toni** resources, supervision, writing-review & editing; **Andrea Di Nisio** resources, supervision, writing-review & editing; **Laura Cendron** conceptualization, project administration, resources, supervision, writing-original draft, writing-review & editing; **Alessandro Angelini** conceptualization, project administration,

https://doi.org/10.1021/acs.chemrestox.2c00211
Chem. Res. Toxicol. XXXX, XXX, XXX−XXX

resources, supervision, writing-original draft, writing-review & editing.

Funding

This research received no external funding.

Notes

The authors declare no competing financial interest.

■ ACKNOWLEDGMENTS

The authors would like to thank the staff of ID23-2 beamline of the European Synchrotron Radiation Facility (ESRF, Grenoble, France) for assistance with crystal testing and data collection.

■ REFERENCES

(1) Evich, M. G.; Davis, M. J. B.; McCord, J. P.; Brad, A.; Awkerman, J. A.; Knappe Detlef, R. U.; Lindstrom, A. B.; Speth, T. F.; Tebes-Stevens, C.; Strynar, M. J.; Wang, Z.; Weber, E. J.; Henderson, M. W.; Washington, J. W. Per- and Polyfluoroalkyl Substances in the Environment. *Science* **2022**, *375*, No. eabg9065.

(2) Dhore, R.; Murthy, G. S. Per/Polyfluoroalkyl Substances Production, Applications and Environmental Impacts. *Bioresour. Technol.* **2021**, *341*, No. 125808.

(3) Kwiatkowski, C. F.; Andrews, D. Q.; Birnbaum, L. S.; Bruton, T. A.; DeWitt, J. C.; Knappe, D. R. U.; Maffini, M. V.; Miller, M. F.; Pelch, K. E.; Reade, A.; Soehl, A.; Trier, X.; Venier, M.; Wagner, C. C.; Wang, Z.; Blum, A. Scientific Basis for Managing PFAS as a Chemical Class. *Environ. Sci. Technol. Lett.* **2020**, *7*, 532−543.

(4) Pan, Y.; Wang, J.; Yeung, L. W. Y.; Wei, S.; Dai, J. Analysis of Emerging Per- and Polyfluoroalkyl Substances: Progress and Current Issues. *TrAC Trends Anal. Chem.* **2020**, *124*, 115481.

(5) Buck, R. C.; Franklin, J.; Berger, U.; Conder, J. M.; Cousins, I. T.; De Voogt, P.; Jensen, A. A.; Kannan, K.; Mabury, S. A.; van Leeuwen, S. P. J. Perfluoroalkyl and Polyfluoroalkyl Substances in the Environment: Terminology, Classification, and Origins. *Integr. Environ. Assess. Manag.* **2011**, *7*, 513−541.

(6) Nakayama, S. F.; Yoshikane, M.; Onoda, Y.; Nishihama, Y.; Iwai-Shimada, M.; Takagi, M.; Kobayashi, Y.; Isobe, T. Worldwide Trends in Tracing Poly- and Perfluoroalkyl Substances (PFAS) in the Environment. *TrAC Trends Anal. Chem.* **2019**, *121*, 115410.

(7) Cordner, A.; De La Rosa, V. Y.; Schaider, L. A.; Rudel, R. A.; Richter, L.; Brown, P. Correction: Guideline Levels for PFOA and PFOS in Drinking Water: The Role of Scientific Uncertainty, Risk Assessment Decisions, and Social Factors. *J. Expo. Sci. Environ. Epidemiol.* **2019**, *29*, 861.

(8) Fiedler, H.; van der Veen, I.; de Boer, J. Global Interlaboratory Assessments of Perfluoroalkyl Substances under the Stockholm Convention on Persistent Organic Pollutants. *TrAC Trends Anal. Chem.* **2020**, *124*, 115459.

(9) DeLuca, N. M.; Angrish, M.; Wilkins, A.; Thayer, K.; Cohen Hubal, E. A. Human Exposure Pathways to Poly- and Perfluoroalkyl Substances (PFAS) from Indoor Media: A Systematic Review Protocol. *Environ. Int.* **2021**, *146*, No. 106308.

(10) Domingo, J. L.; Nadal, M. Per- and Polyfluoroalkyl Substances (PFASs) in Food and Human Dietary Intake: A Review of the Recent Scientific Literature. *J. Agric. Food Chem.* **2017**, *65*, 533−543.

(11) Sunderland, E. M.; Hu, X. C.; Dassuncao, C.; Tokranov, A. K.; Wagner, C. C.; Allen, J. G. A Review of the Pathways of Human Exposure to Poly- and Perfluoroalkyl Substances (PFASs) and Present Understanding of Health Effects. *J. Expo. Sci. Environ. Epidemiol.* **2019**, *29*, 131−147.

(12) Podder, A.; Sadmani, A. H. M. A.; Reinhart, D.; Chang, N.-B.; Goel, R. Per and Poly-Fluoroalkyl Substances (PFAS) as a Contaminant of Emerging Concern in Surface Water: A Transboundary Review of Their Occurrences and Toxicity Effects. *J. Hazard. Mater.* **2021**, *419*, No. 126361.

(13) Emerce, E.; Çetin, Ö. Genotoxicity Assessment of Perfluoroalkyl Substances on Human Sperm. *Toxicol. Ind. Health* **2018**, *34*, 884−890.

(14) Domingo, J. L.; Nadal, M. Human Exposure to Per- and Polyfluoroalkyl Substances (PFAS) through Drinking Water: A Review of the Recent Scientific Literature. *Environ. Res.* **2019**, *177*, No. 108648.

(15) Stahl, T.; Mattern, D.; Brunn, H. Toxicology of Perfluorinated Compounds. *Environ. Sci. Eur.* **2011**, *23*, 38.

(16) Abunada, Z.; Alazaiza, M. Y. D.; Bashir, M. J. K. An Overview of Per- and Polyfluoroalkyl Substances (PFAS) in the Environment: Source, Fate, Risk and Regulations. *Water* **2020**, *12*, 3590.

(17) Li, J.; He, J.; Niu, Z.; Zhang, Y. Legacy Per- and Polyfluoroalkyl Substances (PFASs) and Alternatives (Short-Chain Analogues, F-53B, GenX and FC-98) in Residential Soils of China: Present Implications of Replacing Legacy PFASs. *Environ. Int.* **2020**, *135*, No. 105419.

(18) European Commission. Poly- and Perfluoroalkyl Substances (PFAS): Chemicals Strategy for Sustainability Towards a Toxic-Free Environment. *Common Staff Working Document*, 2020, pp. 1−22.

(19) Ateia, M.; Maroli, A.; Tharayil, N.; Karanfil, T. The Overlooked Short- and Ultrashort-Chain Poly- and Perfluorinated Substances: A Review. *Chemosphere* **2019**, *220*, 866−882.

(20) Munoz, G.; Liu, J.; Vo Duy, S.; Sauvé, S. Analysis of F-53B, Gen-X, ADONA, and Emerging Fluoroalkylether Substances in Environmental and Biomonitoring Samples: A Review. *Trends Environ. Anal. Chem.* **2019**, *23*, No. e00066.

(21) Ruan, T.; Field, J.; Cousins, I.; Lohmann, R.; Jiang, G. Emerging Contaminants: Fluorinated Alternatives to Existing PFAS. *Environ. Sci. Technol.* **2022**, *56*, 6001−6003.

(22) Wang, Z.; DeWitt, J.; Higgins, C. P.; Cousins, I. T. Correction to "A Never-Ending Story of Per- and Polyfluoroalkyl Substances (PFASs)?". *Environ. Sci. Technol.* **2018**, *52*, 3325.

(23) Li, F.; Duan, J.; Tian, S.; Ji, H.; Zhu, Y.; Wei, Z.; Zhao, D. Short-Chain per- and Polyfluoroalkyl Substances in Aquatic Systems: Occurrence, Impacts and Treatment. *Chem. Eng. J.* **2020**, *380*, No. 122506.

(24) Pan, Y.; Zhang, H.; Cui, Q.; Sheng, N.; Yeung, L. W. Y.; Sun, Y.; Guo, Y.; Dai, J. Worldwide Distribution of Novel Perfluoroether Carboxylic and Sulfonic Acids in Surface Water. *Environ. Sci. Technol.* **2018**, *52*, 7621−7629.

(25) Hopkins, Z. R.; Sun, M.; DeWitt, J. C.; Knappe, D. R. U. Recently Detected Drinking Water Contaminants: GenX and Other Per- and Polyfluoroalkyl Ether Acids. *J. AWWA* **2018**, *110*, 13−28.

(26) Rice, P. A.; Cooper, J.; Koh-Fallet, S. E.; Kabadi, S. V. Comparative Analysis of the Physicochemical, Toxicokinetic, and Toxicological Properties of Ether-PFAS. *Toxicol. Appl. Pharmacol.* **2021**, *422*, No. 115531.

(27) Mullin, L.; Katz, D. R.; Riddell, N.; Plumb, R.; Burgess, J. A.; Yeung, L. W. Y.; Jogsten, I. E. Analysis of Hexafluoropropylene Oxide-Dimer Acid (HFPO-DA) by Liquid Chromatography-Mass Spectrometry (LC-MS): Review of Current Approaches and Environmental Levels. *TrAC Trends Anal. Chem.* **2019**, *118*, 828−839.

(28) ECHA. Acetic acid, 2,2-difluoro-2-[[2,2,4,5-tetrafluoro-5-(trifluoromethoxy)-1,3-dioxolan-4-yl]oxy]- ammonium salt (1:1) https://echa.europa.eu/it/registration-dossier/-/registered-dossier/5712.

(29) Bao, Y.; Deng, S.; Jiang, X.; Qu, Y.; He, Y.; Liu, L.; Chai, Q.; Mumtaz, M.; Huang, J.; Cagnetta, G.; Yu, G. Degradation of PFOA Substitute: GenX (HFPO−DA Ammonium Salt): Oxidation with UV/Persulfate or Reduction with UV/Sulfite? *Environ. Sci. Technol.* **2018**, *52*, 11728−11734.

(30) Zhang, S.; Chen, K.; Li, W.; Chai, Y.; Zhu, J.; Chu, B.; Li, N.; Yan, J.; Zhang, S.; Yang, Y. Varied Thyroid Disrupting Effects of Perfluorooctanoic Acid (PFOA) and Its Novel Alternatives Hexafluoropropylene-Oxide-Dimer-Acid (GenX) and Ammonium 4,8-Dioxa-3H-Perfluorononanoate (ADONA) in Vitro. *Environ. Int.* **2021**, *156*, No. 106745.

(31) Pan, Y.; Qin, H.; Zheng, L.; Guo, Y.; Liu, W. Disturbance in Transcriptomic Profile, Proliferation and Multipotency in Human

https://doi.org/10.1021/acs.chemrestox.2c00211
Chem. Res. Toxicol. XXXX, XXX, XXX−XXX

Mesenchymal Stem Cells Caused by Hexafluoropropylene Oxides. *Environ. Pollut.* **2022**, *292*, No. 118483.
(32) EFSA Panel on on Food Contact Materials Flavourings and Processing Aids (CEF). Scientific Opinion on the Safety Assessment of the Substance, Perfluoro{acetic Acid, 2-[(5-Methoxy-1, 3-Dioxolan-4-Yl)Oxy]}, Ammonium Salt, CAS No 1190931-27-1, for Use in Food Contact Materials. *EFSA J.* **2014**, *12*, 3718.
(33) Coperchini, F.; Croce, L.; Ricci, G.; Magri, F.; Rotondi, M.; Imbriani, M.; Chiovato, L. Thyroid Disrupting Effects of Old and New Generation PFAS. *Front. Endocrinol.* **2021**, *11*, No. 612320.
(34) De Toni, L.; Di Nisio, A.; Rocca, M. S.; Pedrucci, F.; Garolla, A.; Dall'Acqua, S.; Guidolin, D.; Ferlin, A.; Foresta, C. Comparative Evaluation of the Effects of Legacy and New Generation Perfluoralkyl Substances (PFAS) on Thyroid Cells In Vitro. *Front. Endocrinol.* **2022**, *13*, 15096.
(35) Gomis, M. I.; Vestergren, R.; Borg, D.; Cousins, I. T. Comparing the Toxic Potency in Vivo of Long-Chain Perfluoroalkyl Acids and Fluorinated Alternatives. *Environ. Int.* **2018**, *113*, 1−9.
(36) Li, Y.; Andersson, A.; Xu, Y.; Pineda, D.; Nilsson, C. A.; Lindh, C. H.; Jakobsson, K.; Fletcher, T. Determinants of serum half-lives for linear and branched perfluoroalkyl substances after long-term high exposure—A study in Ronneby, Sweden. *Environ. Int.* **2022**, *163*, No. 107198.
(37) Fu, J.; Gao, Y.; Cui, L.; Wang, T.; Liang, Y.; Qu, G.; Yuan, B.; Wang, Y.; Zhang, A.; Jiang, G. Occurrence, Temporal Trends, and Half-Lives of Perfluoroalkyl Acids (PFAAs) in Occupational Workers in China. *Sci. Rep.* **2016**, *6*, 38039.
(38) Forsthuber, M.; Kaiser, A. M.; Granitzer, S.; Hassl, I.; Hengstschläger, M.; Stangl, H.; Gundacker, C. Albumin Is the Major Carrier Protein for PFOS, PFOA, PFHxS, PFNA and PFDA in Human Plasma. *Environ. Int.* **2020**, *137*, No. 105324.
(39) Lu, Y.; Meng, L.; Ma, D.; Cao, H.; Liang, Y.; Liu, H.; Wang, Y.; Jiang, G. The Occurrence of PFAS in Human Placenta and Their Binding Abilities to Human Serum Albumin and Organic Anion Transporter 4. *Environ. Pollut.* **2021**, *273*, No. 116460.
(40) Alesio, J. L.; Slitt, A.; Bothun, G. D. Critical New Insights into the Binding of Poly- and Perfluoroalkyl Substances (PFAS) to Albumin Protein. *Chemosphere* **2022**, *287*, No. 131979.
(41) Chi, Q.; Li, Z.; Huang, J.; Ma, J.; Wang, X. Interactions of Perfluorooctanoic Acid and Perfluorooctanesulfonic Acid with Serum Albumins by Native Mass Spectrometry, Fluorescence and Molecular Docking. *Chemosphere* **2018**, *198*, 442−449.
(42) Liu, Y.; Cao, Z.; Zong, W.; Liu, R. Interaction Rule and Mechanism of Perfluoroalkyl Sulfonates Containing Different Carbon Chains with Human Serum Albumin. *RSC Adv.* **2017**, *7*, 24781−24788.
(43) Perera, N. L. D.; Miksovska, J.; O'Shea, K. E. Elucidation of Specific Binding Sites and Extraction of Toxic Gen X from HSA Employing Cyclodextrin. *J. Hazard. Mater.* **2022**, *425*, No. 127765.
(44) Delva-Wiley, J.; Jahan, I.; Newman, R. H.; Zhang, L.; Dong, M. Computational Analysis of the Binding Mechanism of GenX and HSA. *ACS Omega* **2021**, *6*, 29166−29170.
(45) Maso, L.; Trande, M.; Liberi, S.; Moro, G.; Daems, E.; Linciano, S.; Sobott, F.; Covaceuszach, S.; Cassetta, A.; Fasolato, S.; Moretto, L. M.; De Wael, K.; Cendron, L.; Angelini, A. Unveiling the Binding Mode of Perfluorooctanoic Acid to Human Serum Albumin. *Protein Sci.* **2021**, *30*, 830−841.
(46) Liberi, S.; Linciano, S.; Moro, G.; De Toni, L.; Cendron, L.; Angelini, A. Structural Analysis of Human Serum Albumin in Complex with the Fibrate Drug Gemfibrozil. *Int. J. Mol. Sci.* **2022**, *23*, 1769.
(47) Chen, R. F. Removal of Fatty Acids from Serum Albumin by Charcoal Treatment. *J. Biol. Chem.* **1967**, *242*, 173−181.
(48) Potterton, L.; Agirre, J.; Ballard, C.; Cowtan, K.; Dodson, E.; Evans, P. R.; Jenkins, H. T.; Keegan, R.; Krissinel, E.; Stevenson, K.; Lebedev, A.; McNicholas, S. J.; Nicholls, R. A.; Noble, M.; Pannu, N. S.; Roth, C.; Sheldrick, G.; Skubak, P.; Turkenburg, J.; Uski, V.; von Delft, F.; Waterman, D.; Wilson, K.; Winn, M.; Wojdyr, M. CCP4i2: The New Graphical User Interface to the CCP4 Program Suite. *Acta Crystallogr. D* **2018**, *74*, 68−84.
(49) McCoy, A. J.; Grosse-Kunstleve, R. W.; Adams, P. D.; Winn, M. D.; Storoni, L. C.; Read, R. J. Phaser Crystallographic Software. *J. Appl. Crystallogr.* **2007**, *40*, 658−674.
(50) Vagin, A. A.; Steiner, R. A.; Lebedev, A. A.; Potterton, L.; McNicholas, S.; Long, F.; Murshudov, G. N. REFMAC5 Dictionary: Organization of Prior Chemical Knowledge and Guidelines for Its Use. *Acta Crystallogr. D* **2004**, *60*, 2184−2195.
(51) Adams, P. D.; Afonine, P. V.; Bunkóczi, G.; Chen, V. B.; Davis, I. W.; Echols, N.; Headd, J. J.; Hung, L.-W.; Kapral, G. J.; Grosse-Kunstleve, R. W.; McCoy, A. J.; Moriarty, N. W.; Oeffner, R.; Read, R. J.; Richardson, D. C.; Richardson, J. S.; Terwilliger, T. C.; Zwart, P. H. PHENIX: A Comprehensive Python-Based System for Macromolecular Structure Solution. *Acta Crystallogr. D* **2010**, *66*, 213−221.
(52) Emsley, P.; Lohkamp, B.; Scott, W. G.; Cowtan, K. Features and Development of Coot. *Acta Crystallogr. D* **2010**, *66*, 486−501.
(53) Laskowski, R. A.; Watson, J. D.; Thornton, J. M. ProFunc: A Server for Predicting Protein Function from 3D Structure. *Nucleic Acids Res.* **2005**, *33*, W89−W93.
(54) Laskowski, R. A.; Swindells, M. B. LigPlot+: Multiple Ligand-Protein Interaction Diagrams for Drug Discovery. *J. Chem. Inf. Model.* **2011**, *51*, 2778−2786.
(55) *The PyMOL Molecular Graphics, Version 2.0*; Schrödinger, LLC
(56) Linciano, S.; Moro, G.; Zorzi, A.; Angelini, A. Molecular Analysis and Therapeutic Applications of Human Serum Albumin-Fatty Acid Interactions. *J. Controlled Release* **2022**, *348*, 115−126.
(57) Allendorf, F.; Berger, U.; Goss, K.-U.; Ulrich, N. Partition Coefficients of Four Perfluoroalkyl Acid Alternatives between Bovine Serum Albumin (BSA) and Water in Comparison to Ten Classical Perfluoroalkyl Acids. *Environ. Sci. Process. Impacts* **2019**, *21*, 1852−1863.
(58) Calafat, A. M.; Kato, K.; Hubbard, K.; Jia, T.; Botelho, J. C.; Wong, L.-Y. Legacy and Alternative Per- and Polyfluoroalkyl Substances in the U.S. General Population: Paired Serum-Urine Data from the 2013-2014 National Health and Nutrition Examination Survey. *Environ. Int.* **2019**, *131*, No. 105048.
(59) Zorzi, A.; Linciano, S.; Angelini, A. Non-Covalent Albumin-Binding Ligands for Extending the Circulating Half-Life of Small Biotherapeutics. *Medchemcomm* **2019**, *10*, 1068−1081.
(60) Blake, E.; Harlie Cope, A.; Hall Samantha, M.; Keys Robert, D.; Mahler Beth, W.; McCord, J.; Brittany, S.; Stapleton Heather, M.; Strynar Mark, J.; Elmore Susan, A.; Fenton Suzanne, E. Evaluation of Maternal, Embryo, and Placental Effects in CD-1 Mice Following Gestational Exposure to Perfluorooctanoic Acid (PFOA) or Hexafluoropropylene Oxide Dimer Acid (HFPO-DA or GenX). *Environ. Health Perspect.* **2020**, *128*, 27006.
(61) Caverly Rae, J. M.; Craig, L.; Slone, T. W.; Frame, S. R.; Buxton, L. W.; Kennedy, G. L. Evaluation of Chronic Toxicity and Carcinogenicity of Ammonium 2,3,3,3-Tetrafluoro-2-(Heptafluoropropoxy)-Propanoate in Sprague−Dawley Rats. *Toxicol. Rep.* **2015**, *2*, 939−949.

https://doi.org/10.1021/acs.chemrestox.2c00211
Chem. Res. Toxicol. XXXX, XXX, XXX−XXX

Supporting Information

Investigation of the interaction between human serum albumin and branched short-chain perfluoroalkyl compounds

Giulia Moro[1,3], Stefano Liberi[2,†], Filippo Vascon[2], Sara Linciano[1], Sofia De Felice[2], Silvano Fasolato[3], Carlo Foresta[4], Luca De Toni[4], Andrea Di Nisio[4], Laura Cendron[2], Alessandro Angelini[1,5*]*

[1] Department of Molecular Sciences and Nanosystems, Ca' Foscari University of Venice, Via Torino 155, 30172 Venice, Italy

[2] Department of Biology, University of Padua, Viale G. Colombo 3, 35131 Padua, Italy

[3] Department of Medicine, University of Padua, Via Giustiniani 2, 35128 Padova, Italy

[4] Department of Medicine, Unit of Andrology and Reproductive Medicine, University of Padua, Via Giustiniani 2, 35128 Padua, Italy

[5] European Centre for Living Technology (ECLT), Ca' Bottacin, Dorsoduro 3911, Calle Crosera, 30123 Venice, Italy

* Authors to whom correspondence should be addressed: laura.cendron@unipd.it and alessandro.angelini@unive.it

† Present address: The Armenise-Harvard Laboratory of Structural Biology, Department of Biology and Biotechnology “L. Spallanzani”, University of Pavia, Via Ferrata 9, 27100 Pavia, Italy.

Table of contents:

Table S1. Statistics on X-ray diffraction data collection and refinement. A single crystal was used to collect all diffraction data. Highest-resolution shell statistics are shown within brackets.

Data collection *	**hSA-HPFO-DA-Myr**
Beamline	ID 23-2
Wavelength (Å)	0.8731
Space group	C 1 2 1
Cell parameters	
a, *b*, *c* (Å); α, β, γ (°)	185.89 38.77 96.45 90 105.0 90
Resolution (Å)	93.16 – 2.2 (2.28 – 2.2)
Unique observations	34368 (3431)
Multiplicity	5.5 (5.6)
R_{merge}	0.079 (0.78)
R_{pim}	0.036 (0.219)
<I / σ(I)>	14.3 (2.27)
CC1/2	0.998 (0.81)
Completeness (%)	99.70 (99.77)
Refinement	
No. reflections (used for R_{free} calculation)	34341 (1715)
R_{work} / R_{free}	0.237 / 0.259

Number non-hydrogen atoms	4830
protein (chain A)	4643
ligands (HPFO-DA, Myr, Br)	153
solvent	34
Geometry	
RMSD values	
bond lengths (Å)	0.013
bond angles (°)	1.55
Ramachandran plot (%)	
most favored	97.06
additionally allowed	2.76
outliers	0.17
Average B-factor	50.66

Table S2. Atoms of HPFO-DA forming inter-molecular polar and non-polar interactions with atoms and residues of hSA (PDB ID: 7Z57). Optimal inter-molecular hydrogen bonds (HB) and polar interactions (PI) were defined using PROFUNC [1] and LIGPLOT+ [2]. Not specified interactions are non-polar. Interactions have distances shorter than 4.0 Å.

Binding site	hSA atom / residue	atom, interaction, distance (Å)	
		HPFOA-DA1	HPFOA-DA2
FA4	NH1 / Arg410	F18 (PI, 3.68)	
	OH / Tyr411	F19 (HB, 2.54)	
	OH / Tyr411	C03 (3.73)	
	OH / Tyr411	F15 (PI, 3.86)	
	OH / Tyr411	F16 (PI, 3.42)	
	OH / Tyr411	F19 (PI, 2.54)	
	CE1 / Tyr411	F19 (3.45)	
	CZ / Tyr411	F19 (3.35)	
	O / Leu430	F14 (PI, 3.85)	
	CB / Leu430	F15 (3.71)	
	CD2 / Leu430	F15 (3.60)	
	NE / Arg485		O20 (HB, 2.85)
	NH2 / Arg485		O20 (HB, 2.87)
	CD / Arg485	O20 (3.33)	

	CB / Arg485		F19 (3.83)
	CB / Arg485		O20 (3.89)
	CG / Arg485		F15 (3.48)
	CG / Arg485		O08 (3.79)
	CD / Arg485		C10 (3.70)
	CD / Arg485		F15 (3.08)
	CD / Arg485		F16 (3.31)
	CD / Arg485		O08 (3.72)
	NE / Arg485		C01 (3.64)
	NE / Arg485		C03 (3.85)
	NE / Arg485		C10 (3.59)
	NE / Arg485		F15 (PI, 3.47)
	NE / Arg485		F16 (PI, 2.88)
	NE / Arg485		O08 (PI, 3.32)
	NE / Arg485		O20 (PI, 2.85)
	CZ / Arg485		F16 (3.03)
	CZ / Arg485		O20 (3.27)
	NH1 / Arg485		F16 (PI, 3.52)
	NH2 / Arg485		C01 (3.76)
	NH2 / Arg485		F16 (PI, 3.48)

	NH2 / Arg485		O20 (PI, 2.87)
	CB / Phe488	F06 (3.85)	
	N / Ser489	F06 (PI, 3.85)	
	CA / Ser489	O02 (3.71)	
	CB / Ser489	O02 (3.50)	
	CB /Ser489	O20 (3.88)	
	OG / Ser489	C01 (3.02)	
	OG / Ser489	F06 (PI, 3.39)	
	OG / Ser489	O02 (PI, 2.96)	
	OG / Ser489	O20 (PI, 2.67)	
FA3	OG / Ser342		F06 (HB, 3.34)
	OG / Ser342		O02 (HB, 2.91)
	CB / Ser342		C04 (3.75)
	CB / Ser342		F06 (3.21)
	CB / Ser342		F07 (3.25)
	CB / Ser342		O02 (3.73)
	OG / Ser342		F06 (PI, 3.34)
	OG / Ser342		F07 (PI, 3.55)
	OG / Ser342		O02 (PI, 2.91)
	CG2 / Val344		C01 (3.76)

	CG2 / Val344		F07 (3.06)
	CG2 / Val344		O02 (3.40)
	NH1 / Arg348		O20 (HB, 3.33)
	NH2 / Arg348		O20 (HB, 2.62)
	CZ / Arg348		O20 (3.39)
	NH1 / Arg348		C01 (3.80)
	NH1 / Arg348		O02 (PI, 3.35)
	NH1 / Arg348		O20 (PI, 3.33)
	NH2 / Arg348		C01 (3.48)
	NH2 / Arg348		O02 (PI, 3.71)
	NH2 / Arg348		O20 (PI, 2.62)
	O / Pro384		F14 (PI, 3.14)
	CB / Pro384		F17 (3.40)
	CB / Leu387		F13 (3.51)
	CG / Leu387		F13 (3.35)
	CD2 / Leu387	O20 (3.47)	F13 (3.34)
	CD2 / Leu387		F16 (3.55)
	N / Ile388		F14 (PI, 3.84)
	CG1 / Ile388		C11 (3.72)
	CG1 / Ile388		F12 (3.82)

	CG1 / Ile388		F14 (2.79)
	CD1 / Ile388		F14 (3.23)
	CB / Asn391	F12 (3.53)	
	CG / Asn391	F12 (3.71)	
	OD1 / Asn391	F16 (PI, 3.84)	
	ND2 / Asn391	F12 (PI, 3.87)	
	ND2 / Asn391	F18 (PI, 3.85)	
	CD2 / Leu407	F16 (3.67)	
	O / Met446		F05 (PI, 3.80)
	O / Met446		F06 (PI, 3.68)
	CG / Met446		F06 (3.01)
	C / Ala449		F05 (3.43)
	O / Ala449		F05 (PI, 3.89)
	CB / Ala449		F05 (3.65)
	CB / Ala449		F12 (3.61)
	CB / Ala449		F18 (3.26)
	N / Glu450		F05 (PI, 2.99)
	CA / Glu450		F05 (3.10)
	CA / Glu450		F07 (3.69)
	CB / Glu450		C04 (3.78)

	CB / Glu450		F05 (3.45)
	CB / Glu450		F07 (3.19)
	CG / Glu450		F07 (3.46)
	CD / Glu450		F07 (3.78)
	CD1 / Leu453		F05 (3.87)
	CD1 / Leu453		F15 (3.18)
	CD1 / Leu453		O08 (3.83)

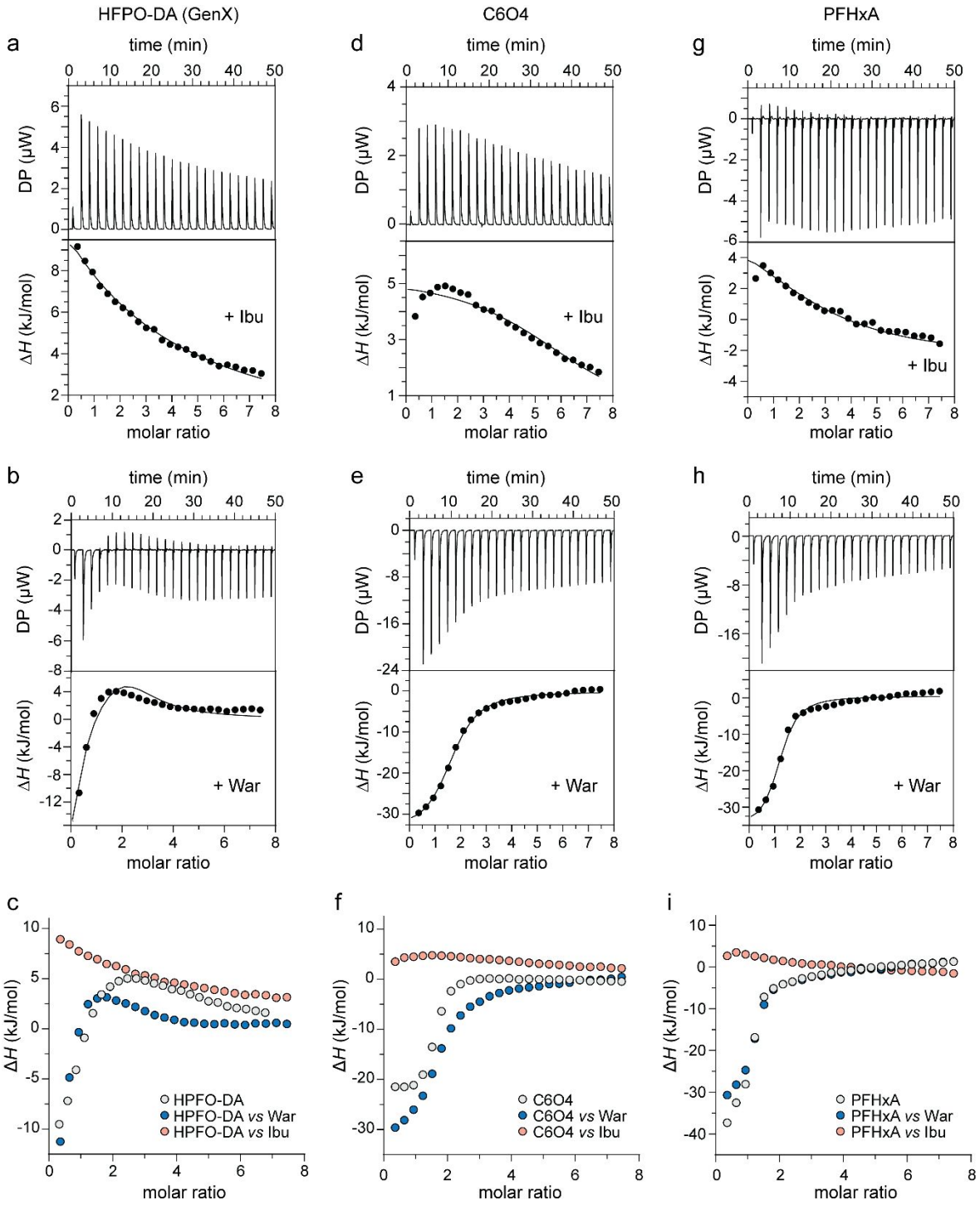

Figure S1. Isothermal titration calorimetry analysis of defatted hSA to HPFO-DA, C6O4 and PFHxA in the presence of hSA-binding drugs ibuprofen (Ibu) or warfarin (War) at 298 K. Representative raw trace (top) and integrated binding isotherm (bottom) of the calorimetric titration of HPFO-DA (**a-b**), C6O4 (**d-e**) and PFHxA (**g-h**). Single titration profiles of C6O4

(**c**), PFHxA (**f**) and HPFO-DA (**i**) in absence of competitors (light grey), in the presence of ibuprofen (Ibu, light red) or in the presence of warfarin (War, light blue).

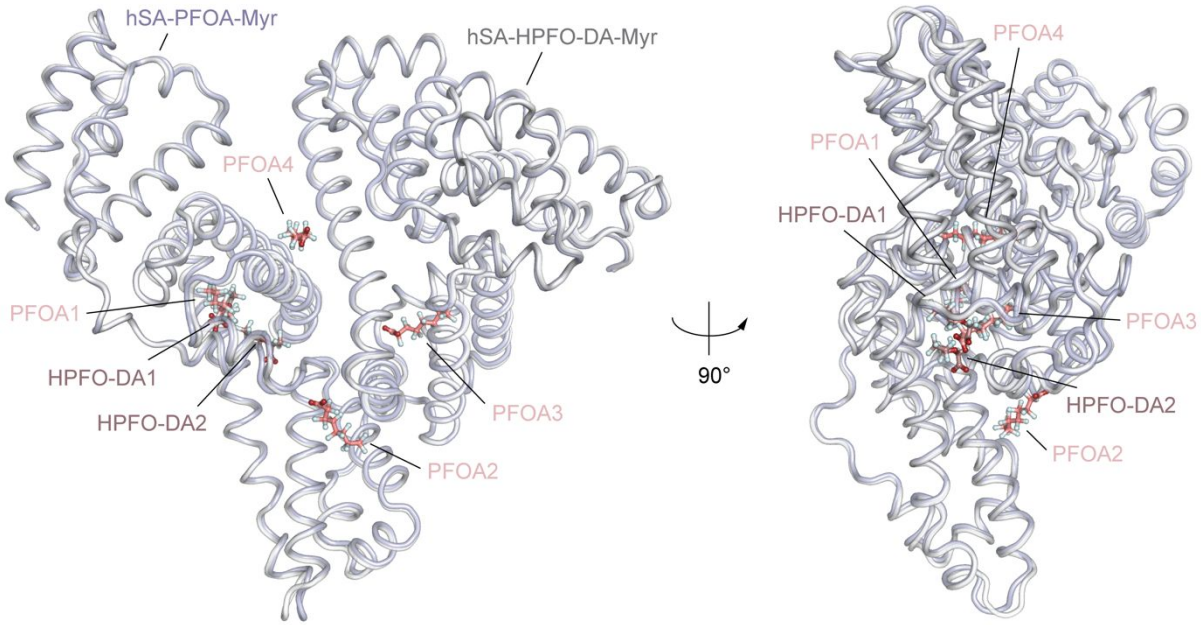

Figure S2. Superimposition of hSA-HPFO-DA-Myr [PDB ID: 7Z57] and hSA-PFOA-Myr [PDB ID: 7AAI] complexes. The overlaid α-helices of hSA-HPFO-DA-Myr (white, dirty violet) and hSA-PFOA-Myr (light blue, dark salmon) complexes are shown by ribbon diagrams and in two orientations (90˚ rotation). The three-dimensional superimposed structures were generated and rendered using PYMOL [3].

References

(1) Laskowski, R. A.; Watson, J. D.; Thornton, J. M. ProFunc: A Server for Predicting Protein Function from 3D Structure. *Nucleic Acids Res.* **2005**, *33* (suppl_2), W89–W93. https://doi.org/10.1093/nar/gki414.

(2) Laskowski, R. A.; Swindells, M. B. LigPlot+: Multiple Ligand-Protein Interaction Diagrams for Drug Discovery. *J. Chem. Inf. Model.* **2011**, *51*, 2778–2786. https://doi.org/10.1021/ci200227u.

(3) The PyMOL Molecular Graphics System, Version 2.0 Schrödinger, LLC.